Layer Korringa-Kohn-Rostoker technique for surface and interface electronic properties

J. M. MacLaren
Theoretical Division, Los Alamos National Laboratory, Los Alamos, New Mexico 87545

S. Crampin, D. D. Vvedensky, and J. B. Pendry
The Blackett Laboratory, Imperial College, London SW7 2BZ, United Kingdom
(Received 13 February 1989)

A technique is presented for embedding planar defects such as interfaces or surfaces in an otherwise perfect crystal. The method is a layer Korringa-Kohn-Rostoker scheme, in which a solid containing the defect is first partitioned into layers of atoms. The scattering properties of each layer are calculated in a partial-wave basis set, using the two-dimensional symmetry assumed to be present in each layer. The layers are subsequently coupled together, in a plane-wave basis, to form a solid. The self-consistent equations for the scattering matrices of semi-infinite bulk regions embedding the defect are solved iteratively, removing the constraint of three-dimensional translational symmetry. Within this formalism, "supercell" and "slab" boundary conditions can also be applied with no extra difficulty. The approach is illustrated in detail for a twin fault in aluminum, for which the microscopic origins of the stacking-fault properties are discussed. Changes in local symmetry and the resulting hybridization of electronic states explain the observed perturbations in the stacking-fault electronic structure.

I. INTRODUCTION

The number of surface or interface atoms where the potential shows appreciable deviation from bulk forms a small percentage of the total in a real crystal. However, defects such as surfaces and interfaces often play a prominent role in determining the chemical and physical properties of materials. For example, catalytic activity depends crucially on the precise nature and position of surface atoms and coadsorbates and the nature of electronic states associated with the surface.[1] Interfaces, such as stacking faults and grain boundaries, are important in determining many mechanical properties such as deformation behavior[2] as well as corrosion resistance and resistivity.[3] In addition, segregated impurities play as important a role as modifiers of interfacial properties,[4] as do their counterparts catalyst poisons and promoters.[5] As a result there has been much work recently in both the development of techniques capable of accurate first-principles calculations of such systems and in the innovative use of traditional bulk-electronic-structure approaches to these complex problems.[6]

Calculations of surface and interface electronic properties with accuracy comparable to those of bulk techniques have only been realized of late. The problems associated with the reduced symmetry, and the effectively infinite number of unique atoms, have lead many authors to impose the somewhat artificial "slab" or "supercell" boundary conditions. The former have almost exclusively been used for surface calculations,[7] where a film of a finite number of layers of atoms is chosen to represent the desired system.[8] There have been many successful film calculations of surface electronic structure and the properties of coadsorbates on a wide range of substrates. Examples include studies of localized surface states on Al(100),[9,10] the interactions between Ni, CO, and coadsorbed promoters and poisons,[11] and the electronic structure of actinide surfaces.[12] The supercell boundary condition has been predominantly used for interface calculations. The region of interest containing the defect is periodically repeated along the $\hat{\mathbf{z}}$ direction,[13] hence making the system a bulk calculation at the expense of a large number of atoms in the unit cell. The properties of a Si grain boundary[14] and Si stacking faults[15] have been treated this way using a pseudopotential approach. The imposition of these boundary conditions does have certain disadvantages, namely localized states induced by the defect may interact between adjacent supercells or in film calculations surface states from either side of the film may couple. In the example of an aluminum surface calculation by Chelikowsky *et al.*,[16] possible localized surface states were observed which decayed by only about 10% from the surface value at the center of a 13-layer film.

Recent interest in the physical properties of interfaces has stemmed from their importance in determining the mechanical behavior of many materials. For example, ductility in intermetallic Al-based alloys may be improved by segregated impurities.[17] The high stacking-fault energies generally observed in these intermetallics tend to prevent slip and thus results in poor ductility. The calculation of stacking-fault electronic properties, and the modification by impurities, is therefore of considerable technological interest since experimental alloy development programs are expensive and time consuming. Theoretical alloy development along these lines is now being actively researched by several groups.[17,18]

The problem of treating a real surface was first ad-

dressed in the pioneering work of Appelbaum and Hamann.[19] Their approach was to match surface and bulk wave functions at a plane inside the bulk by using a transfer-matrix method. Silicon surfaces were treated in this way using a pseudopotential basis set, but there are difficulties associated with the infinite number of bulk states projected onto the two-dimensional (2D) surface band structure. This point is discussed in Inglesfield and Benesh.[20] Wave-function matching of spherical waves was proposed by Holzwarth and Lee,[21] thus allowing transition-metal surface electronic properties to be calculated. The philosophy is essentially the same as Appelbaum and Hamann[19] and so is prone to the same problems.

A more satisfactory way of handling the matching is via the use of Green's functions. This approach has been adopted by several groups. The tight-binding (TB) formalism of Tersoff and Falicov[22] was developed to treat a semi-infinite surfaces and interfaces and subsequently applied to a study of surface and interface magnetism. A Green's-function matching formalism for treating embedded defects has been proposed by Garcia-Moliner and Velasco[23] which could in principle be evaluated in some suitable basis set. Inglesfield[24] has developed a similar Green's function matching formalism in a series of papers, in which he showed that the result of embedding a region in another could be reduced to a surface integral over the bounding surface. These ideas also do not specify the kind of basis set, and Benesh and Inglesfield[20,25] implemented the theory within the linearized augmented-plane-wave (LAPW) basis set and have applied the theory to a study of simple metal surfaces. The LAPW basis allows the full crystal potential to be handled, however since the embedding potential is complex and energy dependent, the principle advantage of linearization, namely reduction to an eigenvalue problem, is lost. Lambrecht and Andersen[26] have calculated the Green's function and hence the electronic structure of an ideal surface using the tight-binding linearized muffin-tin-orbital (TB-LMTO) formalism. Since the TB-LMTO basis functions are short ranged, the semi-infinite nature of the surface could be accounted for in the method, which was applied to a study of Cu(100) and Ge(110) surfaces. An alternative localized basis set was used in the matrix Green's-function formalism[27] by Feibelman[28] in his study of the chemisorption of an isolated Si atom to an Al surface. Podloucky *et al.*[29] have used a similar philosophy to formulate the perturbation due to an impurity substituted in an otherwise perfect lattice. Using a Korringa-Kohn-Rostoker (KKR) basis set the problem of local moment formation in a nonmagnetic hosts was studied within this framework. Thus, the Green's-function approach is a powerful and flexible method for handling perturbations to the perfect crystal.

Theories which use a mixed basis set of partial waves as in the KKR method and plane waves between layers of atoms are collectively known as layer KKR methods. The theories of low-energy electron diffraction (LEED)[30,31] and photoemission[32] use these ideas to couple a bulklike region to the surface. Non-self-consistent surface electronic structure based on LKKR schemes have been reported in the literature by several groups.[33] Multiple-scattering theories of surface and interface electronic structure have been formulated by us[34,35] and other groups.[33,36,37] These methods are easier to implement than Inglesfield's embedding technique and though present calculations have only been performed within KKR basis sets and the muffin-tin approximation to the crystal potential, work is underway to remove this restriction.[38]

In this paper we outline a technique for self-consistent surface or interface electronic-structure calculations using multiple-scattering theory. We believe that we are the first to implement a LKKR approach self-consistently. The theory is first presented in operator formalism, which makes the overall philosophy easier to read. The equations derived are suitable for calculation of matrix elements, which we do in Sec. IV.

II. THE LAYER KORRINGA-KOHN-ROSTOKER APPROACH

The layer Korringa-Kohn-Rostoker (LKKR) method provides a computationally efficient method for calculating self-consistent electronic properties of bulk materials and their interfaces and surfaces. Within the model, real interfaces and surfaces composed of effectively an infinite number of distinct atoms can be treated as easily as interfaces, and surfaces composed of a finite number of atoms build as either a slab or periodically repeated to form a supercell. The only symmetry required is periodicity in two dimensions so that the electronic states can be labelled by a 2D crystal momentum $\mathbf{k}$. Consider as an example an interface between two bulk crystals such as found at stacking faults or grain boundaries. In the LKKR method the system is partitioned into layers of atoms, and then further divided into three regions (see Fig. 1): an interface region containing N_i layers of atoms, and two bulk regions surrounding the interface layers. In the case of a surface calculation one of the bulk regions

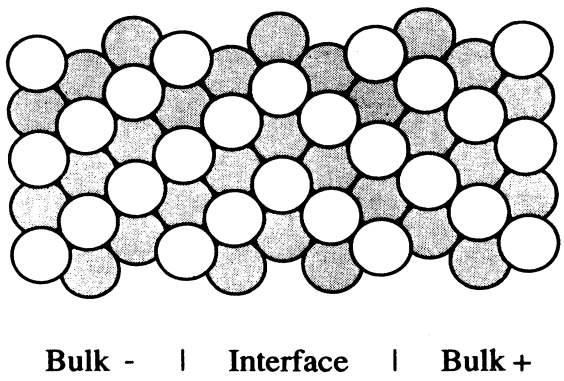

FIG. 1. Atomic geometry of a (111) twin stacking fault in an fcc material, showing the interface embedded in two semi-infinite bulk regions.

would be replaced by vacuum incorporating the surface barrier. The bulk calculation or "supercell" boundary condition can easily be imposed by periodically repeating the interface or surface region and replacing the surrounding bulk, or bulk and vacuum regions with this periodic interface or surface. In a similar manner the slab boundary conditions can be achieved by replacing the bulk regions by vacuum, giving two surface barriers one on either side of the slab.

At the interface, only the potentials on the N_i interfacial layers are allowed to vary during the course of a calculation. The constraint that the atoms in the bulklike regions have fixed potentials allows the scattering properties of the bulk to be built up recursively and is essential for removing the 3D unit cell necessary for treating the isolated interface embedded in the solid in a computationally feasible manner. In the corresponding surface calculation the vacuum region, surface barrier, as well as the surface layers N_s are allowed to relax and only the one set of bulk potentials is kept constant. In practice the number of varying layers will change from system to system and the accuracy of the approximation that all the atoms in the assigned bulk layers have the same potentials can only be checked by repeating the calculation with more varying layers. In metallic systems only a few varying layers are typically required (three to five usually suffices) due to screening of electronic perturbations. In systems where the screening is weak many layers may be needed. However, Inglesfield and Benesh[20] and Crampin *et al.*[35] have found that it is generally the case that as a result of the correct treatment of the boundary conditions fewer layers are required than in the corresponding slab or supercell calculation where there can be significant coupling between the artificially introduced boundaries. The accuracy of the solution can be systematically checked by increasing the size of the interface region.

The calculation of the electronic properties of the system proceeds by finding the energy resolved local density of states (LDOS) $\rho(\mathbf{r},E)$ for the interface or surface region within the one-electron approximation. This is found in an angular momentum representation about each unique atom in the interface or surface region. The LDOS is first related to the imaginary part of the one-electron Green's function

$$\rho(\mathbf{r},E)=-\frac{1}{\pi}\mathrm{Im}G(\mathbf{r},\mathbf{r},E)\ , \tag{1}$$

where E can be complex. Atomic units in which $\hbar=e=m=1$ are used throughout. In this system the unit of energy is the hartree (1 hartree$\simeq$27.2 eV). The ground-state charge density is found from integrals of the Green's functions and then, from density functional theory,[39] self-consistent potentials, charge densities, total energies, pressures, elastic constants, and other physical properties can be calculated. The Green's function is analytic in the upper half of the complex energy plane, which is used to advantage in evaluating many of the integrals needed in the LKKR scheme. The next section is devoted to the calculation of G for a layered system.

III. EVALUATION OF THE GREEN'S FUNCTION

In evaluating G we adopt a multiple-scattering approach in which the scattering paths are separated into inter- and intralayer scattering events, of which the former are summed in a recursive manner. In keeping with other KKR-based multiple-scattering theories,[31,33,40] the crystal potential is replaced by the approximate muffin-tin form, where the potential within touching atomic spheres is replaced by its spherical average and in the interstitial region by a constant which is the volume average over this region. In contrast to KKR theories though, the usual separation between structure and potential is only partial. The time-consuming 2D structure constants for each layer, which sum intralayer scattering paths, separate from the potential, but the construction of the scattering operators for the semi-infinite bulk regions, which sum interlayer scattering, mix both structure and potential.

The scattering path operator τ, originally introduced by Beeby[41] and generalized by Gyorffy,[42] provides the simplest way of summing the scattering paths, and we adopt this approach and the notation of Faulkner and Stocks[40] (FS) in the derivation of the Green's functions. The resulting expressions are simplified by utilizing the 2D translational symmetry present within each layer of atoms, and leads to a $\mathbf{k}$-resolved Green's function which must be integrated over the 2D Brillouin zone (BZ). Since the Green's function is always evaluated at energy E, for notational convenience the energy variable will not be written.

We start with the familiar Dyson equation for the Green's function of the solid G,

$$G=G_0+G_0TG_0\ , \tag{2}$$

where G_0 is the free-space Green's function satisfying

$$G_0(\mathbf{r},\mathbf{r}')=G_0(\mathbf{r}-\mathbf{r}') \tag{3}$$

and T is the scattering operator for the whole solid. The Green's function will be cast in form suitable for expansion about a particular layer i. To achieve this T is expressed as a sum of the scattering-path operators for all the atoms in the solid as

$$T=\sum_{\alpha,\beta}\tau^{\alpha\beta}\ , \tag{4}$$

where these operators satisfy the following equations of motion

$$\begin{aligned}\tau^{\alpha\beta}&=t^{\alpha}\delta_{\alpha\beta}+t^{\alpha}G_0\sum_{\gamma\neq\alpha}\tau^{\gamma\beta}\ ,\\ \tau^{\alpha\beta}&=t^{\alpha}\delta_{\alpha\beta}+\sum_{\gamma\neq\beta}\tau^{\alpha\gamma}G_0t^{\beta}\ .\end{aligned} \tag{5}$$

t^{α} is the isolated atomic-scattering operator, and α, β, and γ refer to atomic sites. $\delta_{\alpha\beta}$ is the usual Kronecker δ function. After some manipulation, described in FS, one gets the following expression for the Green's function about site α in terms of the atomic Green's function for that site G^{α} and the operator $T^{\alpha\alpha}$ which sums all scattering events which neither begin nor end on the site α,

$$G=G^{\alpha}+G^{\alpha}T^{\alpha\alpha}G^{\alpha} \tag{6}$$

with

$$T^{\alpha\alpha}=\sum_{\beta\neq\alpha,\gamma\neq\alpha}\tau^{\beta\gamma} \tag{7}$$

and

$$G^{\alpha}=G_0+G_0t^{\alpha}G_0 \ . \tag{8}$$

The form of (6) is to be expected, since about site α the full and atomic Green's functions satisfy the same differential equation and differ only in boundary conditions. The change in the boundary condition when the atom is embedded in the solid is reflected by the second term in this equation. Further manipulation of (6) leads to

$$G=G^{\alpha}+(1+G_0t^{\alpha})(t^{\alpha})^{-1}(\tau^{\alpha\alpha}-t^{\alpha})(t^{\alpha})^{-1}(1+t^{\alpha}G_0) \ . \tag{9}$$

Equation (9) is the operator equivalent of FS's Eq. (2.18) and is valid for any set of nonoverlapping scatterers. At this stage it is convenient to make use of the 2D translational symmetry present in this particular case. The equations of motion then satisfied by the scattering-path operators remain essentially the same, except that the free-space Green's function is replaced by the 2D Bloch Green's function g, where

$$\mathcal{G}(\mathbf{R})=\sum_{J}{}' G_0(\mathbf{R}+\mathbf{R}_J)e^{i\mathbf{k}\cdot\mathbf{R}_J} \ . \tag{10}$$

The prime on the summation is taken to exclude the $J=0$ term only when $|\mathbf{R}|=|\mathbf{r}-\mathbf{r}'|=0$. The τ operators now depend on $\mathbf{k}$ and *only* couple unique atoms in the 2D unit cell, and the vectors $\mathbf{R}_J$ are the 2D real-space lattice vectors. Equation (9) now becomes

$$G=G^{\alpha}+(1+G_0t^{\alpha})(t^{\alpha})^{-1}\left[\frac{1}{\Omega}\int_{\Omega}\tau^{\alpha\alpha}(\mathbf{k})d\mathbf{k}-t^{\alpha}\right]\times(t^{\alpha})^{-1}(1+t^{\alpha}G_0) \ , \tag{11}$$

where Ω is the area of the 2D BZ. We now perform a resummation of the paths in $\tau^{\alpha\alpha}$ showing explicitly the embedding of layer i in the host and introducing quantities suitable for computation. To do this we introduce new scattering path operators τ_i, which sums all scattering paths which *end* with a scattering event within layer i, and τ_L and τ_R which sum those paths ending with a scattering event within the left and right half-spaces (i.e., all layers up to but excluding layer i from either side). These operators have an implicit $\mathbf{k}$ dependence which we omit from the expressions. Clearly the sum of all three operators includes all possible scattering paths,

$$T=\tau_L+\tau_i+\tau_R \ . \tag{12}$$

We denote by T_i the scattering operator of layer i and by T_L^{i-1} and T_R^{i+1} the scattering operators of the left and right half-spaces, where these operators sum all paths *within* the relevant subspace. In terms of these quantities, the τ operators satisfy the following equations of motion:

$$\begin{aligned}\tau_L&=(1+\tau_i\mathcal{G}+\tau_R\mathcal{G})T_L^{i-1} \ ,\\ \tau_i&=(\tau_L\mathcal{G}+1+\tau_R\mathcal{G})T_i \ ,\\ \tau_R&=(\tau_L\mathcal{G}+\tau_i\mathcal{G}+1)T_R^{i+1} \ .\end{aligned} \tag{13}$$

Manipulation of these equations gives

$$\begin{aligned}\tau_R&=(1+T_L^i\mathcal{G})T_R^{i+1}(1-\mathcal{G}T_L^i\mathcal{G}T_R^{i+1})^{-1} \ ,\\ \tau_L&=(1+T_R^i\mathcal{G})T_L^{i-1}(1-\mathcal{G}T_R^i\mathcal{G}T_L^{i-1})^{-1}\end{aligned} \tag{14}$$

from which τ_i is given by

$$\tau_i=[1+(1+T_L^i\mathcal{G})T_R^{i+1}(1-\mathcal{G}T_L^i\mathcal{G}T_R^{i+1})^{-1}\mathcal{G}+(1+T_R^i\mathcal{G})T_L^{i-1}(1-\mathcal{G}T_R^i\mathcal{G}T_L^{i-1})^{-1}\mathcal{G}]T_i \ , \tag{15}$$

where we have used the fact that (see Appendix A)

$$\begin{aligned}T_L^i&=T_i+(1+T_i\mathcal{G})T_L^{i-1}(1-\mathcal{G}T_iT_L^{i-1})^{-1}(1+\mathcal{G}T_i) \ ,\\ T_R^i&=T_i+(1+T_i\mathcal{G})T_R^{i+1}(1-\mathcal{G}T_i\mathcal{G}T_R^{i+1})^{-1}(1+\mathcal{G}T_i)\end{aligned} \tag{16}$$

in simplifying the algebra. The scattering operator for an isolated layer T_i may be found by a 2D Fourier transform of (5) where the sites that appear are restricted to atomic sites in the layer unit cell. This is directly analogous to the calculation of the bulk T matrix in standard 3D KKR theory. The resulting expression is

$$T_i=(t^{-1}-\mathcal{G})^{-1} \ . \tag{17}$$

Having obtained this, we can now write down the expression for τ_i which we have found most convenient for computation,

$$\tau_i=T_i+T_iR_i^{\text{eff}}T_i \ , \tag{18}$$

where R_i^{eff}, the effective reflectivity of the solid excluding layer i is given by

$$\begin{aligned}R_i^{\text{eff}}=&[1+T_R^{i+1}(1-\mathcal{G}T_i\mathcal{G}T_R^{i+1})^{-1}(1+\mathcal{G}T_i)\mathcal{G}]\\ &\times T_L^{i-1}(1-\mathcal{G}T_R^i\mathcal{G}T_L^{i-1})^{-1}\mathcal{G}\\ &+[1+T_L^{i-1}(1-\mathcal{G}T_i\mathcal{G}T_L^{i-1})^{-1}(1+\mathcal{G}T_i)\mathcal{G}]\\ &\times T_R^{i+1}(1-\mathcal{G}T_L^i\mathcal{G}T_R^{i+1})^{-1}\mathcal{G} \ .\end{aligned} \tag{19}$$

The second term in (18) corrects for the embedding of layer i in the host crystal. Evaluating the effective reflectivity is the most demanding stage in the calculation of the Green's function. The half-space operators can be found from the two-center formulas in Appendix A, summarized by

$$T_{12}=(1-T_1\mathcal{G}T_2\mathcal{G})^{-1}T_1(1+\mathcal{G}T_2)+(1-T_2\mathcal{G}T_1\mathcal{G})^{-1}T_2(1+\mathcal{G}T_1) \tag{20}$$

through the use of layer doubling and layer coupling algorithms,[43] details of which are given in the next section. The formal solution for the E-resolved Green's function for an atom in a layer embedded in a host crystal is given by (11), where the site diagonal blocks of τ are most easily found from (18).

IV. IMPLEMENTATION

In this part of the paper we will calculate the matrix elements of the scattering operators introduced in Sec. III, necessary for the evaluation of the Green's function of the solid.

A. Scattering by the isolated muffin tin

The solutions to the isolated muffin tin needed for constructing the atomic Green's function and t matrix are found in the usual way. Since this theory is well known we refer the reader to Refs. 32, 40–42, or 44 for a discussion of scattering from an isolated muffin-tin potential.

B. Scattering by an isolated layer

The intralayer scattering is also expressed solely in the angular momentum basis set. Taking matrix elements of T_i in (17) gives

$$[T_i^{-1}]_{LL'}^{\alpha_i\beta_i} \equiv \langle L\alpha_i | T_i^{-1} | L'\beta_i \rangle = (t_l^{\alpha_i})^{-1}\delta_{\alpha_i\beta_i}\delta_{LL'} - \langle L\alpha_i | \mathcal{G} | L'\beta_i \rangle \ . \quad (21)$$

The angular momentum matrix elements of g are the 2D KKR structure constants.[45] These Green's functions have real- and reciprocal-space representations. The latter can be shown to be uniformly convergent for $z > 0$, and this forms the basis for coupling the layers together (Sec. IV C). However, for small and zero z, the expansion is too slowly converging and has to be calculated by an Ewald approach by partitioning into convergent real- and reciprocal space summations. The derivation is complicated and details of this along with all the various expansions of g are given in a series of papers by Kambe,[45,46] to which we refer the reader. This work is a generalization to 2D of the work of Ham and Segall.[47]

C. Coupling layers

All the layers are coupled together in a plane-wave basis. Thus terms in (15) which correspond to interlayer scattering will be solved in this basis set and then transformed back into the angular momentum basis set. The plane-wave basis functions are given in a coordinate representation by

$$\langle \mathbf{r} | \mathbf{K}_{\mathbf{g}}^{\pm} \rangle = e^{i\mathbf{K}_{\mathbf{g}}^{\pm}\cdot\mathbf{r}} \ , \quad (22)$$

where

$$\mathbf{K}_{\mathbf{g}}^{\pm} = \begin{cases} \mathbf{k}+\mathbf{g} \pm \sqrt{2E - |\mathbf{k}+\mathbf{g}|^2}\,\hat{\mathbf{z}}, & 2E > |\mathbf{k}+\mathbf{g}|^2 \\ \mathbf{k}+\mathbf{g} \pm i\sqrt{|\mathbf{k}+\mathbf{g}|^2 - 2E}\,\hat{\mathbf{z}}, & 2E < |\mathbf{k}+\mathbf{g}|^2 \ . \end{cases} \quad (23)$$

The $\pm$ refers to the propagation direction in the $\hat{\mathbf{z}}$ direction, and as one goes out in the 2D reciprocal lattice with increasing $|\mathbf{g}|$, $\mathbf{K}_{gz}$ has an increasing imaginary component with the result that the amplitude of the basis vector on the next layer becomes increasingly less important. This attenuation allows a truncation of the basis set after only a modest number of vectors, typically 10–20. Within the plane-wave basis, inclusion of scattering by complete layers of atoms is achieved by the introduction of four operators $T_i^{\pm\pm}$ representing reflection from or transmission through either side of layer i [see Fig. 2(a)], where

$$\begin{aligned} T_i^{-+} &= \Gamma^- T_i \tilde{\Gamma}^+, \quad T_i^{++} = 1 + \Gamma^+ T_i \tilde{\Gamma}^+ \ , \\ T_i^{+-} &= \Gamma^+ T_i \tilde{\Gamma}^-, \quad T_i^{--} = 1 + \Gamma^- T_i \tilde{\Gamma}^- \ . \end{aligned} \quad (24)$$

$\Gamma^{\pm}$ project incident plane waves into an angular momentum basis in which the intralayer-scattering paths may be summed before projecting back into plane waves with $\tilde{\Gamma}^{\pm}$,

$$\begin{aligned} \Gamma_i^{\pm gL} &= 4\pi i^l (-1)^m e^{i\mathbf{K}_{\mathbf{g}}^{\pm}\cdot\mathbf{r}_{\beta_i}} Y_{l,-m}(\mathbf{K}_{\mathbf{g}}^{\pm}) \ , \\ \tilde{\Gamma}_i^{\pm Lg} &= \frac{2\pi i^{-l}}{\kappa A (K_{\mathbf{g}}^{+})_z} e^{-i\mathbf{K}_{\mathbf{g}}^{\pm}\cdot\mathbf{r}_{\beta_i}} Y_{l,m}(\mathbf{K}_{\mathbf{g}}^{\pm}) \ . \end{aligned} \quad (25)$$

It is most convenient to evaluate the scattering matrices (24) for each layer with reference to an origin within that layer, which makes it necessary to introduce propagators to translate the origin. Within the plane-wave basis the propagators translating the origin from layer i to layer $i+1$ and vice versa are denoted by $P_i^{\pm}$ which are, in fact, just the plane-wave matrix elements of the Bloch Green's function g

$$P_{i\mathbf{g}\mathbf{g}'}^{\pm} = \langle \mathbf{K}_{\mathbf{g}}^{\pm} | g | \mathbf{K}_{\mathbf{g}'}^{\pm} \rangle = \delta_{\mathbf{g}\mathbf{g}'} e^{i\mathbf{K}_{\mathbf{g}}^{\pm}\cdot(\mathbf{c}_{i+1}-\mathbf{c}_i)} \ , \quad (26)$$

where $\mathbf{c}_i$ is the origin of layer i. Using these propagators and the layer scattering matrices it is also possible to describe the total scattering by two layers by T operators, found by coupling together the individual $T_i^{\pm\pm}$ in the following manner [see Fig. 2(b)]:

$$\begin{aligned} T_{1,2}^{++} &= T_1^{++}(1 - P_1^+ T_2^{+-} P_1^- T_1^{-+})^{-1} P_1^+ T_2^{++} \ , \\ T_{1,2}^{--} &= T_2^{--}(1 - P_1^- T_1^{-+} P_1^+ T_2^{+-})^{-1} P_1^- T_1^{--} \ , \\ T_{1,2}^{+-} &= T_1^{+-} + T_1^{++} P_1^+ T_2^{+-} \\ &\quad \times (1 - P_1^- T_1^{-+} P_1^+ T_2^{+-})^{-1} P_1^- T_1^{--} \ , \\ T_{1,2}^{-+} &= T_2^{-+} + T_2^{--} P_1^- T_1^{-+} \\ &\quad \times (1 - P_1^+ T_2^{+-} P_1^- T_1^{-+})^{-1} P_1^+ T_2^{++} \ . \end{aligned} \quad (27)$$

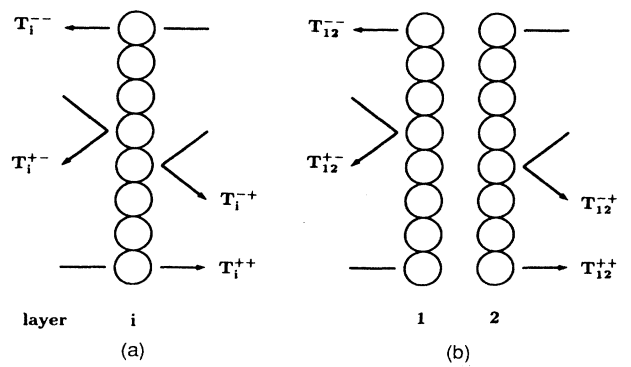

FIG. 2. Schematic illustration of (a) the four-layer scattering matrices for layer i—T_i^{++}, T_i^{+-}, T_i^{-+}, and T_i^{--}—and (b) the four coupled layer matrices T_{12}^{++}, T_{12}^{+-}, T_{12}^{-+}, and T_{12}^{--}.

These are just the plane-wave matrix elements of the two-center scattering equations given in Appendix A. Further layers may be incorporated into this scheme by treating $T_{1,2}^{\pm\pm}$ as a single layer, and solving Eqs. (27) with the substitutions $T_1^{\pm\pm}\rightarrow T_{1,2}^{\pm\pm}$, $T_2^{\pm\pm}\rightarrow T_3^{\pm\pm}$, and $P_1^{\pm}\rightarrow P_2^{\pm}$ to give $T_{1,3}^{\pm\pm}$. Repeated application of this procedure eventually assembles the full three-dimensional solid by stacking one layer at a time. In the case where similar units of layers are involved this calculation may be greatly accelerated by a technique known as layer doubling.[43] Such a situation arises within the layers on either side of the interface region, where semi-infinite periodicity exists. Bulk scattering operators are found first by building the repeat unit of layers for the relevant half-space using equations (27). Then, setting both $T_1^{\pm\pm}$ and $T_2^{\pm\pm}$ equal to the scattering matrices of this repeat unit a larger repeat unit may be found by again solving (27). Recursive application of this algorithm using the scattering matrices of the previous "double" assembles the layers at an exponential rate rather than linear as simple application of (27) achieves.

D. Matrix elements of τ

In determining τ_i, the reflection operators of the two half-spaces are required. These are simply

$$\langle \mathbf{K}_{\mathbf{g}}^{-}|T_L^i|\mathbf{K}_{\mathbf{g}'}^{+}\rangle=[T_{-\infty}^{-+}]_{\mathbf{g}\mathbf{g}'}\ ,$$
$$\langle \mathbf{K}_{\mathbf{g}}^{+}|T_R^i|\mathbf{K}_{\mathbf{g}'}^{-}\rangle=[T_{i,\infty}^{+-}]_{\mathbf{g}\mathbf{g}'}\ . \tag{28}$$

To simplify notation in the rest of this section we introduce $R_i^L=P_i^- T_{-\infty,i}^{-+}$ and $R_i^R=P_{i-1}^+ T_{i,\infty}^{+-}$. The determination of these matrices assumes that the layer-coupling scheme will converge after the incorporation of a finite number of layers. In general this is not guaranteed at real energies, where an extended Bloch state may propagate to the furthest layer included, scatter into another extended state, and propagate back. It is therefore necessary to introduce a small imaginary component into the energy which results in all states decaying in a finite length and so ensures the convergence of the half-space reflection matrices after a finite number of layers. We illustrate this in Fig. 3 for Ni where the convergence of the doubling algorithm is measured by the largest relative change S_n in any element of the bulk reflection matrix between the nth and $(n-1)$th doubling,

$$S_n=\max\left[\frac{|R_{\mathbf{g}\mathbf{g}'}^{L,n}-R_{\mathbf{g}\mathbf{g}'}^{L,n-1}|}{|R_{\mathbf{g}\mathbf{g}'}^{L,n-1}|}\right], \tag{29}$$

where the superscript n is the result of the reflection matrix after n "layer doubles." We note that at a real energy where an extended Bloch state exists no convergence is obtained even after the inclusion of 2×10^6 layers. The addition of a small imaginary component ($E_i=10^{-5}$ hartree) to the energy is seen to produce convergence, and after 18 layer doublings S_n is less than 10^{-30}. Similar convergence is rapidly obtained even at real energies provided there are no travelling Bloch states present.

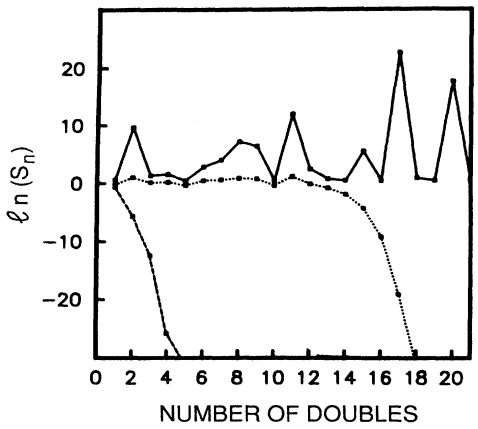

FIG. 3. Graph showing the convergence, monitored by S_n (defined in Sec. IV C), of the layer doubling algorithm for bulk Ni along the (111) direction. The solid line shows the behavior of S_n in the presence of an extended state. The dotted line indicates convergence is obtained when $E_i=10^{-5}$. The dashed line is evaluated where $E_i=0$ and *no* extended state exists and also shows convergence.

In terms of the left and right space reflectivities R_i^{eff} is given by

$$\langle L\alpha_i|R_i^{\text{eff}}|L'\beta_i\rangle=\langle L\alpha_i|[\tilde{\Gamma}-R_{i-1}^L+\tilde{\Gamma}^+(1-R_{i+1}^R P_i^- T_i^{-+})^{-1}R_{i+1}^R P_i^- T_i^{--}R_{i-1}^L](1-R_i^R R_{i-1}^L)^{-1}P_{i-1}^+\Gamma^+$$
$$+[\tilde{\Gamma}^+R_{i+1}^R+\tilde{\Gamma}^-(1-R_{i-1}^L P_{i-1}^+ T_i^{+-})^{-1}R_{i-1}^L P_{i-1}^+ T_i^{++}R_{i+1}^R](1-R_i^L R_{i+1}^R)^{-1}P_i^-\Gamma^-|L'\beta_i\rangle\ , \tag{30}$$

where the terms above correspond to the possible directions of the outgoing and incoming waves arising from multiple scattering with the rest of the solid. Combining this expression for R_i^{eff} with (18) gives site diagonal matrix elements of τ_i. The Green's function at energy E and crystal momentum $\mathbf{k}$ is found from the matrix elements of (11), where we identify

$$R_L^{\alpha_i}(\mathbf{r})=\langle L\alpha_i|1+G_0 t^{\alpha_i}|\mathbf{r}\rangle \tag{31}$$

which is the regular solution to the Schrödinger equation for the isolated muffin-tin formed as the product of the solution to the radial equation and a spherical harmonic. Thus we arrive at the central equation for the LKKR Green's function, namely

$$G(\mathbf{r},\mathbf{r}')=-4i\kappa\sum_L \tilde{R}_L^{\alpha_i}(\mathbf{r}_<)R_L^{(1)\alpha_i}(\mathbf{r}_>)-\frac{4i\kappa}{\Omega}\sum_{LL'}R_L^{\alpha_i}(\mathbf{r}')(t_l^{\alpha_i})^{-1}\left[\int_\Omega d\mathbf{k}\,\tau_{iLL'}^{\alpha\alpha}(\mathbf{k})-\delta_{LL'}t_{l'}^{\alpha_i}\right](t_{l'}^{\alpha_i})^{-1}\tilde{R}_{L'}^{\alpha_i}(\mathbf{r}) \tag{32}$$

where $\mathbf{r}_>/\mathbf{r}_<$ the greater/lesser of $\mathbf{r}$ and $\mathbf{r}'$. $R_L^{(1)\alpha_i}(\mathbf{r}_>)$ is the corresponding irregular solution to the isolated muffin tin. The tilde has been used to denote a complex conjugate of the spherical harmonic only. The matrix elements of τ_i are given in terms of R_i^{eff} by

$$\tau_{iLL'}^{\alpha\alpha}=\langle L\alpha_i(T_iR_i^{\text{eff}}+1)T_i|L'\alpha_i\rangle \ . \tag{33}$$

V. BAND STRUCTURES

The partitioning of the system into layers provides a method for the calculation of the bulk band structure $\mathbf{K}(E)$ both on the real-$\mathbf{K}$ axis of conventional calculations *and* into the complex plane where information regarding the nature of localized states may be found. Wood and Pendry[36] have shown that the 3D band structure can be found from an eigenvalue problem by applying a Bloch condition on the wave functions on either side of the bulk repeat layers. In systems of reduced symmetry for which the LKKR approach has been developed, the bulk band structure is projected onto a 2D analogue. The infinite repeat distance in the $\hat{\mathbf{z}}$ direction results in a BZ with no $\mathbf{K}_z$ dimension. This projected band structure (PBS) is important for the electronic description of both surfaces and interfaces, allowing an identification of regions of E-$\mathbf{K}$ space where extended states exist and hence pointing out pockets where localized states may be present.

Within the LKKR formalism the PBS may be obtained by attempting to converge the bulk reflection matrices on the real-energy axis using the iterative layer doubling method. This procedure fails to converge whenever there is an extended Bloch state present, thus the PBS may be mapped out by noting at which given E and $\mathbf{k}$ points the bulk reflection matrices fail to converge. This also enables a search for localized states to be made. For a given interface, areas of E-$\mathbf{k}$ are identified where no extended states occur. In these regions the reflection matrices $T_{-\infty,i}^{-+}$ and $T_{i+1,\infty}^{+-}$ may therefore be calculated, and thus the Green's function for the solid may also be calculated for this particular E and $\mathbf{k}$. If the DOS is calculated from the imaginary part of G, then interface states can be identified as sharp peaks in the $\mathbf{k}$ resolved DOS, which are localized around the interface.

VI. SELF-CONSISTENT SOLUTION

Self-consistent solutions to the one-electron Schrödinger equation are essential to systems where there is charge rearrangement in forming the surface or interface. These solutions are found iteratively as in most other electronic structure techniques by constructing the potential for the next iteration from the charge density found in the calculation. In the LKKR scheme the charge density about each atomic site is found from the trace of the imaginary part of the Green's function using (32) as a suitable expansion. In constructing the total charge density the Green's function is integrated over both E and $\mathbf{k}$. The 2D BZ integration is approximated by Cunningham's algorithm of special points.[48] Since there are many more 3D bands projected into the 2D BZ this approach should have better convergence properties than in three dimensions. The energy integrations which run from $-\infty\rightarrow E_f$ are first split into core and valence contributions, where core is taken to mean a state with negligible dispersion. The former are treated as an atomic calculation while the contribution from the latter can be expressed as an integral from the bottom of the band to E_f. This real energy contour is deformed into the upper half of the complex energy plane where the Green's function is analytic. A schematic diagram of this analytic structure of the Green's function is shown in Fig. 4(a) along with a typical contour. A simple application of Cauchy's theorem shows that the contribution from this deformed contour is the same as that calculated along the real-energy axis provided the new contour begins and ends at the same points, since the Green's function is an analytic function of energy in the upper half-plane. This has the advantage that many fewer energy sampling points are needed, since the Green's function is smoother as a function of energy in the complex plane. This may be seen from the Kramers-Kronig relation[49] in which the Green's function at imaginary energy E_i is given by the convolution of a Lorentzian with the Green's function evaluated at $E_i=0$. Hence one obtains broadening of the order of E_i in the structure of the Green's function,

$$\text{Im}G(\mathbf{r},\mathbf{r}';E_r+iE_i)=\frac{1}{\pi}\int_{-\infty}^{\infty}dE_r'\frac{E_i}{(E_r-E_r')^2+E_i^2}\text{Im}G(\mathbf{r},\mathbf{r}';E_r') \ . \tag{34}$$

We sample the contour with a Gaussian integration technique which never samples the end points of the contour (hence avoiding any problems at $E_i=0$), and so provides a fast and accurate calculation of the valence charge density. In addition the new contour also improves the accuracy of the BZ sampling, since this algorithm is more effective for smoother charge densities. Typically eight energy and six to ten special $\mathbf{k}$ points are sufficient to converge self-consistent charge densities.

The new potential is constructed from the calculated charge density as a sum of a Coulomb contribution arising from a solution to Poisson's equation and the exchange-correlation potential.[50] In order to prevent instabilities arising from the strength of the Coulomb potential a small amount of the calculated potential is mixed with the potential of the previous input to form the potential for the next iteration. The Coulomb potential, within the muffin-tin approximation, is given for site α_i by

$$V_c^{\alpha_i}(r)=-\frac{z_{\alpha_i}}{r}+\frac{4\pi}{r}\int_0^r r'^2\rho(r')_{\alpha_i}dr'+4\pi\int_r^{R_{\text{MT}}^{\alpha_i}}r'\rho(r')_{\alpha_i}dr'+V^{\alpha_i} \ , \tag{35}$$

where z_{α_i} is the nuclear charge, and V^{α_i} the boundary condition on the atom resulting from the long-range Madelung sum due to all the other atoms (see Appendix B).

Once the self-consistent solutions have been found, the electronic total energy and pressure can be computed.

We have found that calculating the total energy from the sum of kinetic, Coulomb, and exchange correlation, as outlined in Skriver,[51] is numerically more stable than using the simplification scheme suggested by Janak,[52] though we use the core cancellation suggested by Janak in the pressure calculation.

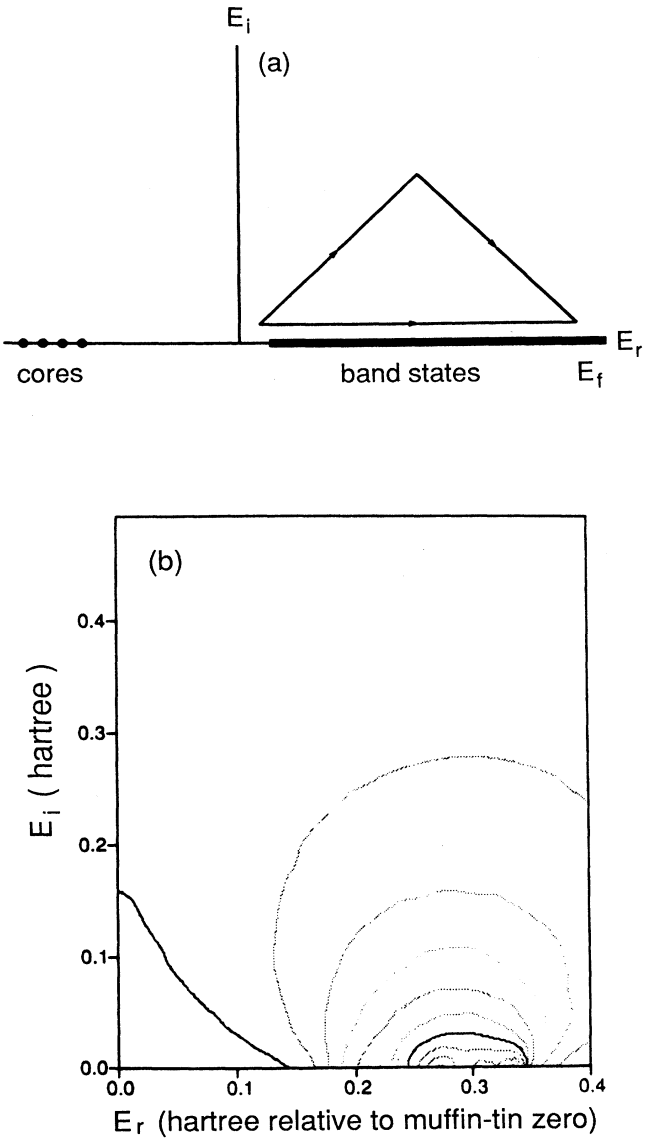

FIG. 4. (a) The analytic structure of the one-electron Green's function in the complex energy plane showing poles at the core eigenvalues and a branch cut corresponding to band states. The charge density follows from an integration of the Green's function along a contour parallel to the real-energy axis, which in the calculation is deformed into the triangular contour. (b) Contour plot of the MTDOS for bulk Ni in the complex energy plane. The contour values are uniformly spaced in steps of 6.5 electrons/hartree. The first contour value is at 6.5 electrons/hartree. Above the real energy axis the MTDOS is a much smoother function.

VII. APPLICATION TO A TWIN FAULT IN ALUMINUM

In this section we will apply the formalism described in the previous sections to a twin fault in aluminum. This defect is formed along the [111] direction of fcc Al by reversing the $\cdots ABCABC \cdots$ stacking sequence to form a locally hcp environment which is $\cdots ABCABACBA \cdots$. This structure is illustrated in Fig. 1. In calculating the electronic properties of the stacking fault we first performed a self-consistent bulk calculation, the results of which were used in constructing the scattering matrices of semi-infinite half-spaces by layer doubling. In the self-consistent calculation the iterations were performed with a basis set that included s, p, and d partial waves ($l=2$), 13 plane waves ($g=13$), eight energy ordinates, and six special **k** points. In evaluating the DOS the energy contour was offset from the real-energy axis by 0.001 hartree, and in this case it was found to be necessary to include 375 **k** points in the $\frac{1}{12}$ irreducible wedge of the BZ to converge the DOS. The fault was modeled with a nine-layer interface region where the potentials were allowed to relax from bulk values embedded in an otherwise perfect host, and no structural relaxation was taken into account. The energy of this twin fault was found to be ~ 120 mJ/m^2,[34] compared to an experimental value of ~ 170 mJ/m^2.[2] The level of agreement is satisfactory since the experimental value is inferred from elasticity theory and miscroscopy measurement and so has a large uncertainty associated with it.

The same size basis sets were chosen for the fault calculation as in the bulk. Each iteration takes approximately 1 h on a VAX 3000 workstation, or 1 min on a CRAY 1-S. The muffin-tin DOS (MTDOS) at the twin fault is shown in Fig. 5. The changes observed in MTDOS are most pronounced on the central-fault layer and heal towards bulk values over the nine-layer interface chosen. These changes can largely be attributed to the change in the environment at the fault, in particular perturbations resulting from hybridization changes in the electronic states arising from the mirror plane. Layers close to the fault show much less structure than the bulk. This is because peaks and troughs in the density-of-states profiles result from critical points in the band structure, some of which arise from the periodicity in the [111]

TABLE I. Peak heights (hartree^{-1}) of the two localized states (s_1 at $\simeq 0.285$ hartree and s_2 at $\simeq 0.31$ hartree) found at the K point as a function of layer. Absolute heights are dependent upon the imaginary energy, due to the Lorentz broadening, but relative heights are not.

Layer	s_1	s_2
1 (sf)	77.6	37.1
2	25.6	121.0
3	37.2	39.1
4	22.0	12.5
5 (bulk)	7.33	39.0

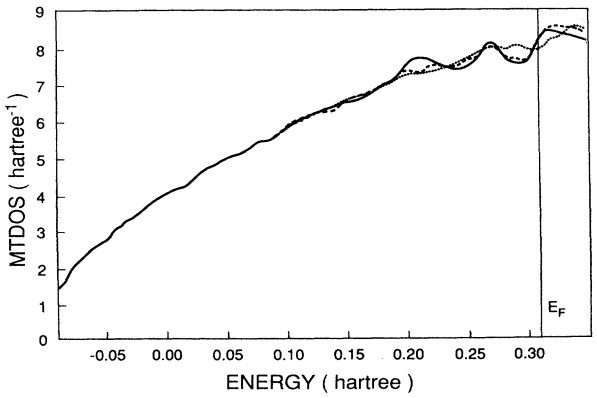

FIG. 5. MTDOS for atoms at an Al(111) twin stacking fault evaluated at 0.001 hartree above the real axis. Shown are the densities of States for the stacking fault layer (· · · ·) the adjacent layer (— — —) and the bulk (——).

direction which is now broken by the fault. States lower down in the band are much more free-electron-like, showing an $E^{1/2}$ behavior, and thus are negligibly perturbed by the fault. In Fig. 6 we show the projected 2D band structure; localized states may exist in the gaps in this band structure. For example, we have located such a state at the **K** point in the 2D zone in the gap where localized surface states have also been found.[10] The MTDOS at the **K** point, Fig. 7, shows the sharp singularities in the DOS at the band edges at $\simeq 0.275$ and $\simeq 0.320$ hartree with respect to the muffin-tin zero. In the gap there are two states seen as sharp peaks in the MTDOS. Neither of the states are strongly localized spatially, and still have significant amplitude on the fifth layer away from the fault. In order to differentiate the spatial decay of the localized states more easily, the peak heights as a function of layer are given in Table I.

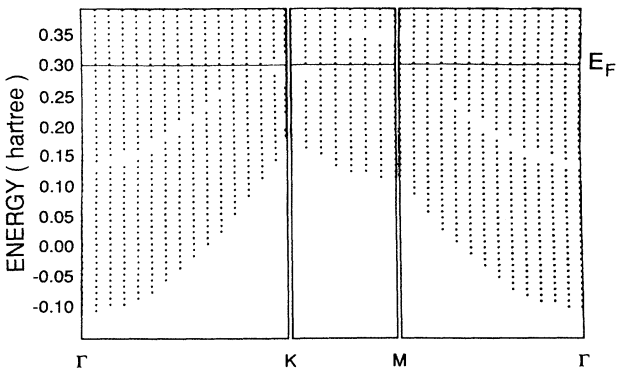

FIG. 6. The 2D projected band structure for the Al(111) twin stacking fault showing gaps where localized states may exist.

VIII. CONCLUSION

In this paper we have described in detail a layer-KKR scheme developed specifically for the correct treatment of a surface or interface embedded in an otherwise perfect host crystal. This embedding is achieved via the recursive calculation of bulk half-space scattering matrices using layer coupling algorithms to avoid the use of a slab or supercell. The approach does, however, have the flexibility to study slabs and supercells if desired and may provide an efficient solution of complicated crystals. We present the first fully self-consistent all-electron calculations of a truly isolated metallic interface, a twin fault in Al, and find that the technique is both accurate, comparable to bulk KKR methods,[53] and computationally fast. The changes in the electronic structure found at the interface are consistent with symmetry considerations at the fault. These perturbations heal slowly into the bulk due to the free-electron nature of the host. At present the technique is being used on both more complicated interfaces and on the role of segregated impurities. These results will be reported elsewhere.[54]

ACKNOWLEDGMENTS

J.M.M. acknowledges support from the U.S. Department of Energy and S.C. from the U.K. Science and Engineering Research Council. D.D.V. and S.C. gratefully acknowledge support from The Office of Naval Research, NATO, and the hospitality of Los Alamos National Laboratory, where some of this work was undertaken.

APPENDIX A: TWO-CENTER SCATTERING FORMULAS

A recurring theme in the derivation of the LKKR equations is the solution of the scattering problem for two scatterers, with scattering operators T_1 and T_2. The resulting scattering operator T_{12} is given by

$$T_{12}=\tau_1+\tau_2 , \tag{A1}$$

where the τ operators satisfy the equations of motion

$$\begin{aligned}\tau_1&=T_1+\tau_2 G_0 T_1 ,\\ \tau_2&=T_2+\tau_1 G_0 T_2 .\end{aligned} \tag{A2}$$

Solving these coupled equations we get the general solution

$$\begin{aligned}T_{12}=&(1-T_1G_0T_2G_0)^{-1}T_1(1+G_0T_2)\\ &+(1-T_2G_0T_1G_0)^{-1}T_2(1+G_0T_1) .\end{aligned} \tag{A3}$$

Written as such T_{12} is in multicenter form, having origins on both scatterer 1 and scatterer 2. Within the layer formalism we find it most convenient to associate with each layer an individual origin. When coupling layers together, for example, the resulting scattering operators have separate origins for incoming and outgoing scattering paths. For computation we manipulate (A3) into the following forms:

$$G_0T_{12}G_0=(1+G_0T_1)(1-G_0T_2G_0T_1)^{-1}\times G_0(1+T_2G_0)-1\ , \tag{A4a}$$

$$G_0T_{12}G_0=(1+G_0T_2)(1-G_0T_1G_0T_2)^{-1}\times G_0(1+T_1G_0)-1\ , \tag{A4b}$$

$$G_0T_{12}G_0=G_0T_1G_0+(1+G_0T_1)G_0T_2(1-G_0T_1G_0T_2)^{-1}\times G_0(1+T_1G_0)\ , \tag{A4c}$$

$$G_0T_{12}G_0=G_0T_2G_0+(1+G_0T_2)G_0T_1(1-G_0T_2G_0T_1)^{-1}\times G_0(1+T_2G_0)\ . \tag{A4d}$$

The Fourier transforms of these equations merely change G_0, the free-space Green's function into $\mathcal{G}$, the Bloch free-space Green's functions. The τ and T operators are then $\mathbf{k}$ resolved.

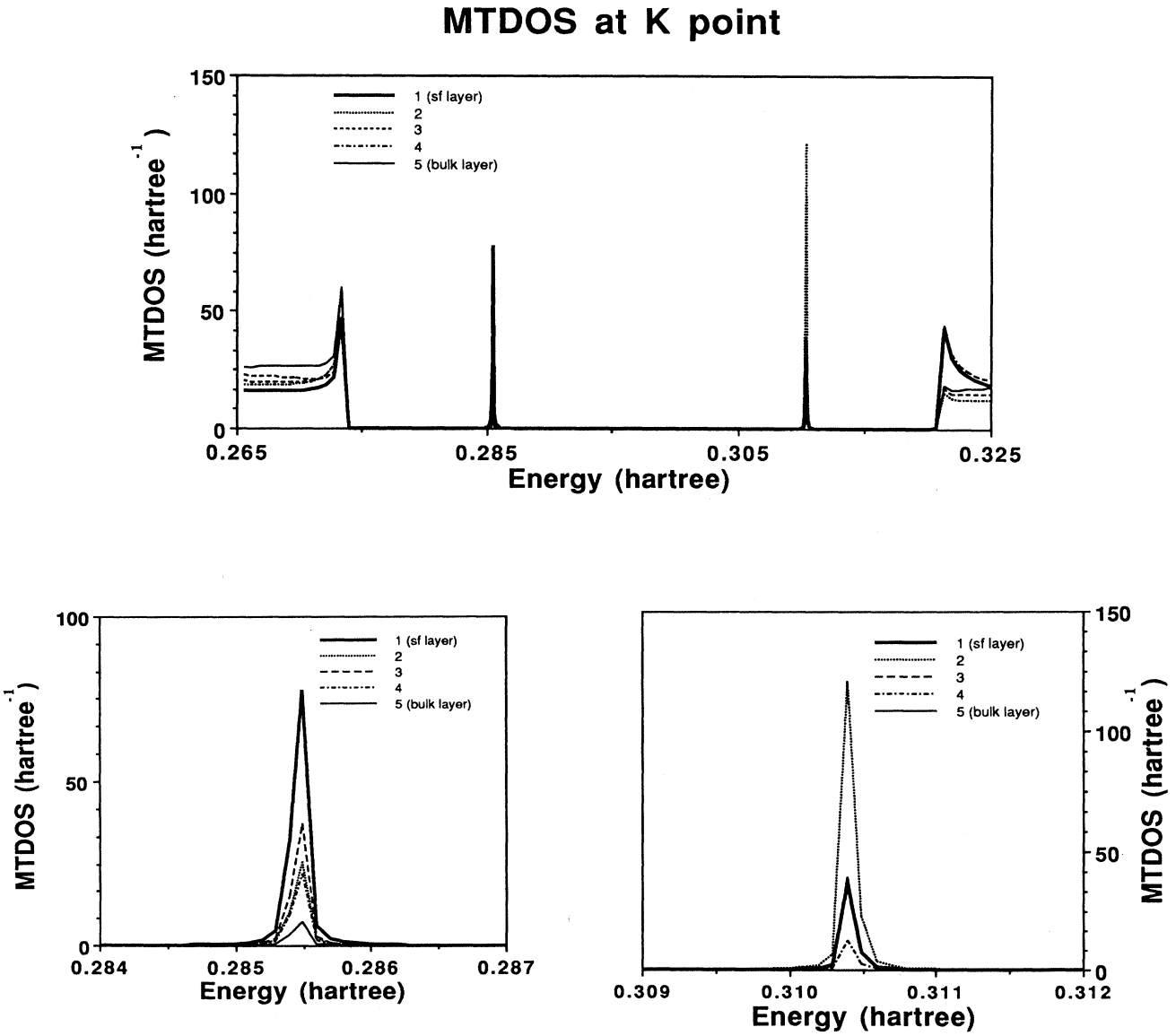

FIG. 7. The MTDOS at the **K** point in the 2D Brillouin zone evaluated at 10^{-6} hartree above the real axis. Note the sharp band edges at $\simeq 0.275$ and $\simeq 0.320$ hartree and the presence of two states in the gap, which are spatially localized on atoms close to the stacking fault.

APPENDIX B: THE SOLUTION OF POISSON'S EQUATION

In solving Poisson's equation, the interstitial charge density is replaced by a constant $\langle\rho\rangle$, determined by the bulk. Thus in the interstitial the potential can be found from the solution to the Ewald problem for a 2D lattice, whose solution can be written formally as

$$V(\mathbf{r})=\frac{2\pi}{\Omega}\int dk_z \sum_{\mathbf{g}} \rho(\mathbf{g},k_z)\frac{e^{i(\mathbf{g}+k_z)\cdot\mathbf{r}}}{(g^2+k_z^2)} . \tag{B1}$$

If $g\neq 0$, then (B1) can be evaluated by contour methods to give

$$V_1(\mathbf{r})=\frac{2\pi}{\Omega}\sum_{\mathbf{g}}{}' \sum_{j\alpha} q_{j\alpha}\frac{e^{i\mathbf{g}\cdot(\mathbf{r}-\mathbf{r}_{j\alpha})}}{g} e^{-g|z-z_{j\alpha}|} . \tag{B2}$$

The summation over α runs over all the atoms in the 2D cells of each layer j. The position of these atoms are denoted by $\mathbf{r}_{j\alpha}$, with a z coordinate of $z_{j\alpha}$. The Ewald lattice has δ-function charges $q_{j\alpha}$ on each of these sites neutralized by the uniform compensating charge of $\langle\rho\rangle$. We have substituted the appropriate Fourier coefficients of such a charge density into (B1) in deriving (B2). The solution to the $\mathbf{g}=0$ is most easily found from the differential equation

$$\frac{d^2V_2(z)}{dz^2}=-\frac{4\pi}{\Omega}[\rho(z)-\langle\rho\rangle\Omega] , \tag{B3}$$

where $\rho(z)$ is the $\mathbf{g}=0$ Fourier coefficient of the charge density. The general solution is

$$V_2(z)=-\frac{4\pi}{\Omega}\left[\sum_{j\alpha} q_{j\alpha}\frac{|z-z_{j\alpha}|}{2}-\Omega\langle\rho\rangle\frac{z^2}{2}+Az+B\right] , \tag{B4}$$

where the j summation is now restricted to the interfacial layers. The last two terms are the solution to Laplace's equation and are fixed by the boundary conditions that the edge atoms outside the interface region are bulklike. In the bulk regions we have

$$V_2(z)=\frac{4\pi}{\Omega}\sum_{g_z}{}' \sum_{j\alpha} g_{j\alpha}\frac{e^{ig_z(z-z_{j\alpha})}}{g_z^2} , \tag{B5}$$

where the j summation runs over all the layers in a bulk cell of length L and the reciprocal lattice vectors are therefore given by $g_z=2\pi i/L$. The summations can be performed since the atoms are periodically arranged on a lattice whose repeat spacing in the z direction is c. Taking the limit $L\rightarrow\infty$ (B5) becomes

$$V_2(z)=\frac{\pi}{\Omega}\sum_{\beta} q_\beta\left[\frac{(z-z_\beta)^2}{2}-2|z-z_\beta|+\frac{c}{3}\right] , \tag{B6}$$

where the sum on β is over the unique atoms in the bulk unit cell.

The boundary conditions on each sphere $V^{\alpha i}$ can now be found as follows. Since the Ewald solution averages to zero over the unit cell, then the appropriate muffin-tin form can be found subtracting from this solution the integral over each muffin-tin sphere. A convenient way of integrating the Ewald solution over the muffin-tin spheres was suggested by Slater and de Cicco.[55] The spherical part of the Coulomb potential, about site α, on the Ewald lattice can be written as

$$V(r)=\frac{q_\alpha}{r}+\frac{2\pi}{3}\langle\rho\rangle r^2+A_\alpha , \tag{B7}$$

which can be trivially integrated over the sphere. The constant A_α is found from the Ewald solution by taking $r\rightarrow 0$ of $V_1(r)+V_2(r)$ [Eqs. (B2) and (B4)] after removing the divergent $1/r$ term.

[1]P. J. Feibelman and D. R. Hamann, Phys. Rev. Lett. **52**, 61 (1984); P. J. Feibelman and D. R. Hamann, Surf. Sci. **149**, 48 (1985); J. M. MacLaren, D. D. Vvedensky, J. B. Pendry, and R. W. Joyner, J. Chem. Soc. Faraday Trans. 1 **83**, 1945 (1987); J. Catal. **110**, 243 (1988).

[2]J. P. Hirth and J. Lothe, *Theory of Dislocations* (McGraw-Hill, New York, 1968); L. E. Murr, *Interfacial Phenomena in Metals and Alloys* (Addison-Wesley, London, 1975).

[3]S. P. Chen, A. F. Voter, and D. J. Srolovitz, Scr. Metall. **20**, 1389 (1986); R. W. Ballufi, *Grain Boundaries Structures and Kinetics* (American Society for Metals, Metals Park, OH, 1980).

[4]G. T. Gray, III, Acta Metall. **36**, 1745 (1988).

[5]D. W. Goodman, Acc. Chem. Res. **17**, 194 (1984).

[6]R. A. de Groot, J. M. Bunting, M. Weger, and F. M. Mueller, Phys. Rev. B **31**, 2881 (1985); F. Springelkamp, R. A. de Groot, W. Geertsma, W. van der Lugt, and F. M. Mueller, *ibid.* **32**, 2319 (1985).

[7]For a review of surface techniques, see, for example, J. E. Inglesfield, Rep. Prog. Phys. **45**, 223 (1982).

[8]W. Kohn, Phys. Rev. B **11**, 3756 (1975); N. Kar and P. Soven, *ibid.* **11**, 3761 (1975); H. Krakauer, M. Posternak, and A. J. Freeman, *ibid.* **19**, 1706 (1979).

[9]H. Krakauer, M. Posternak, and A. J. Freeman, Phys. Rev. Lett. **41**, 1072 (1979).

[10]D. Wang, A. J. Freeman, H. Krakauer, and M. Posternak, Phys. Rev. B **23**, 1685 (1981).

[11]E. Wimmer, C. L. Fu, and A. J. Freeman, Phys. Rev. Lett. **55**, 2618 (1985).

[12]Y. G. Moa, G. W. Fernando, and B. R. Cooper (unpublished).

[13]M. Posternak, H. Krakauer, A. J. Freeman, and D. D. Koelling, Phys. Rev. B **21**, 5601 (1980).

[14]D. P. Di Vincenzo, O. L. Alerhand, M. Schlüter, and J. W. Wilkins, Phys. Rev. Lett. **56**, 1925 (1986).

[15]M. Y. Chou, M. L. Cohen, and S. G. Louie, Phys. Rev. B **32**, 7279 (1986).

[16]J. R. Chelikowsky, M. Schlüter, S. G. Louie, and M. L. Cohen, Solid State Commun. **17**, 1103 (1975).

[17]J.-H. Xu, T. Oguchi, and A. J. Freeman, Phys. Rev. B **36**, 4186 (1987); T. Hong and A. J. Freeman, Mater. Res. Soc. Symp. Proc. **133**, 75 (1989).

[18]M. E. Eberhart and D. D. Vvedensky, Scr. Metall. **22**, 1183 (1988); M. E. Eberhart, M. E. McHenry, and J. M. MacLaren (unpublished).

[19]J. A. Appelbaum and D. R. Hamann, Phys. Rev. B **6**, 2166 (1972).
[20]J. E. Inglesfield and G. Benesh, Phys. Rev. B **37**, 6682 (1988).
[21]N. A. W. Holzwarth and M. J. G. Lee, Phys. Rev. B **18**, 5350 (1978); M. J. G. Lee and N. A. W. Holzwarth, *ibid.* **18**, 5365 (1978).
[22]J. Tersoff and L. M. Falicov, Phys. Rev. B **26**, 6186 (1982).
[23]F. Garcia-Moliner and V. R. Velasco, Prog. Surf. Sci. **21**, 93 (1986).
[24]J. E. Inglesfield, J. Phys. C **14**, 3795 (1981); Surf. Sci. **76**, 355 (1978).
[25]G. Benesh and J. E. Inglesfield, J. Phys. C **17**, 1595 (1984).
[26]W. R. L. Lambrecht and O. K. Andersen, Surf. Sci. **178**, 256 (1986).
[27]A. R. Williams, P. J. Feibelman, and N. D. Lang, Phys. Rev. B **18**, 616 (1978).
[28]P. J. Feibelman, Phys. Rev. Lett. **54**, 2627 (1985).
[29]R. Podloucky, R. Zeller, and P. H. Dederichs, Phys. Rev. B **22**, 5777 (1980).
[30]J. B. Pendry, *Low-Energy Electron Diffraction* (Academic, London, 1974).
[31]A. P. Shen, Phys. Rev. B **12**, 4200 (1972); D. W. Jepsen, P. M. Marcus, and F. Jona, *ibid.* **5**, 3933 (1972).
[32]J. B. Pendry, Surf. Sci. **57**, 679 (1976); J. F. L. Hopkinson, J. B. Pendry, and D. J. Titterington, Comput. Phys. Commun. **19**, 69 (1980).
[33]S. J. Gurman and J. B. Pendry, Phys. Rev. Lett. **31**, 637 (1973); C. Noguerra, D. Spanjaard, and D. W. Jepsen, Phys. Rev. B **17**, 607 (1978); K. Kambe, Surf. Sci. **117**, 443 (1982); G. Wachutka, Phys. Rev. B **36**, 4725 (1987); F. Màca and M. Scheffler, Comput. Phys. Commun. **38**, 403 (1985).
[34]J. M. MacLaren, S. Crampin, D. D. Vvedensky, and M. E. Eberhart, Phys. Rev. Lett. **63**, 2586 (1989).
[35]S. Crampin, D. D. Vvedensky, J. M. MacLaren, and M. E. Eberhart, Mater. Res. Soc. Symp. Proc. **141**, 373 (1989).
[36]K. Wood and J. B. Pendry, Phys. Rev. Lett. **31**, 1400 (1973).
[37]A. Gonis, Phys. Rev. B **34**, 8313 (1985).
[38]A. Gonis, X.-G. Zhang, and D. M. Nicholson, Phys. Rev. B **38**, 3564 (1988).
[39]P. Hohenberg and W. Kohn, Phys. Rev. **136**, 864 (1964); W. Kohn and L. J. Sham, *ibid.* **140**, 1133 (1965).
[40]J. Faulkner and G. M. Stocks, Phys. Rev. B **21**, 3222 (1980).
[41]J. L. Beeby, J. Phys. C **1**, 82 (1968).
[42]B. L. Gyorffy, Phys. Rev. B **5**, 2382 (1972).
[43]A discussion in terms of summing scattering paths can be found in Ref. 30, Chap. 4.
[44]A. Messiah, *Quantum Mechanics* (North-Holland, Amsterdam, 1960); P. Lloyd and P. V. Smith, Adv. Phys. **21**, 69 (1972).
[45]K. Kambe, Z. Naturforsch. **22a**, 322 (1967); **22a**, 422 (1967); **23a**, 1280 (1968).
[46]There are some typographical errors in Kambe's original papers (Ref. 39). The corrections can be found in K. Kambe, Z. Naturforsch. **24c**, 1432 (1969) and on p. 137 of Ref. 30.
[47]F. S. Ham and B. Segall, Phys. Rev. **124**, 1786 (1961).
[48]S. L. Cunningham, Phys. Rev. B **10**, 4988 (1974).
[49]H. Eschrig, R. Richter, and B. Velicky, J. Phys. C **19**, 7173 (1986).
[50]There have been many local-density approximations to the exchange and correlation potential. The one which we have adopted is the Hedin and Lundquist potential, L. Hedin and B. I. Lundquist, J. Phys. C **4**, 2064 (1971).
[51]H. L. Skriver, *The LMTO Method* (Springer-Verlag, New York, 1984).
[52]J. F. Janak, Phys. Rev. B **9**, 3985 (1974).
[53]V. L. Moruzzi, J. F. Janak, and A. R. Williams, *Calculated Electronic Properties of Metals* (Pergamon, New York, 1978).
[54]S. Crampin, D. D. Vvedensky, J. M. MacLaren, and M. E. Eberhart, Phys. Rev. B **40**, 3413 (1989).
[55]J. C. Slater and P. de Cicco, M.I.T. Quarterly Progress Report No. 50, Solid State and Molecular Theory Group, 1963, p. 46 (unpublished).